SPATIAL AND TEMPORAL HETEROGENEITY OF METHANE AND CARBON DIOXIDE PRODUCTION AND FLUX IN A TEMPERATE TIDAL SALT MARSH

by

Frances Bothfeld

A thesis submitted to the Faculty of the University of Delaware in partial fulfillment of the requirements for the degree of Master of Science in Water Science and Policy

Winter 2016

SPATIAL AND TEMPORAL HETEROGENEITY OF METHANE AND CARBON DIOXIDE PRODUCTION AND FLUX IN A TEMPERATE TIDAL SALT MARSH

by

Frances Bothfeld

Approved: _____

Angelia Seyfferth, Ph.D.
Professor in charge of thesis on behalf of the Advisory Committee

Approved: _____

Sheeram Inamdar, Ph.D.
Chair of the Department of Water Science and Policy

Approved: _____

Mark Rieger, Ph.D.
Dean of the College of Agriculture and Natural Resources

Approved: _____

Ann L. Ardis, Ph.D.
Interim Vice Provost for Graduate and Professional Education

ACKNOWLEDGMENTS

I would also like to extend a heartfelt thank you to my committee members, Rodrigo Vargas, Angelia Seyfferth, and Holly Michael for all of their help, this work would not be possible without their guidance. A special thanks goes to the staff of the St. Jones Estuarine Reserve for their support and use of their facilities during the sampling season. This work was also made possible due to the lab assistance provided by Sandra Petrakis, Andrew Morris, Julia Guimond, and the various members of the Seyfferth lab. Nick Kaufman provided data visualization and statistical help as well as overall support. I would also like to thank our funding sources: University of Delaware College of Agriculture and Natural Resources Competitive Seed Grant Program and DNREC.

TABLE OF CONTENTS

LIST OF TABLES

LIST OF FIGURES

ABSTRACT

Salt marshes naturally contribute CO_2 and CH_4 greenhouse gas fluxes to the atmosphere. These fluxes are governed by biogeochemical processes in sediments that are sensitive to local conditions (e.g., temperature, water table fluctuations), which can result in spatial heterogeneity of production and flux in an ecosystem. Therefore, it is critical to understand the driving forces behind CO_2 and CH_4 production and consumption in order to produce accurate estimates of CH_4 and CO_2 contributions to the atmosphere from salt marshes and to understand how it might change with the advent of environmental stressors. In this study, we evaluated the temporal and spatial heterogeneity of biogeochemical cycling of redox-sensitive parameters and CO_2 and CH_4 production and flux in a tidal salt marsh. Two subsites within the marsh with different hydrological regimes were monitored over a one-year period for changes in CO_2 and CH_4 flux to the atmosphere and pore-water chemistry at discrete depths to 90 cm. Additionally, we more intensely monitored CO_2 and CH_4 production with depth and hydrological dynamics at these subsites over one summer month. We found that the subsite proximal to the tidal channel ("near channel subsite") had larger water table elevation fluctuations that resulted in variable, but relatively high, redox values and led to higher CO_2 and typically lower CH_4 fluxes compared to the subsite farther from the tidal channel ("interior subsite"), which experienced a higher water table elevation, more inundation, lower redox values, and lower CO_2 fluxes. The spatial heterogeneity of inundation due to hydrologic factors likely led to differences in dominant soil respiration processes at the two subsites (e.g.,

ix aerobic respiration vs. Fe(III) reduction vs. SO_4^{2-} reduction), which affects the production and flux of CO_2 and CH_4 to the atmosphere. Moreover, the production of these gases with depth revealed a large pool of stored CO_2 and CH_4 gases that has the potential to efflux during land-use change. The interplay of hydrology and sediment biogeochemistry and their effect on spatial heterogeneity in a salt marsh should be considered when attempting to understand the current levels and future dynamics of CO_2 and CH_4 fluxes from salt marshes.

Chapter 1

INTRODUCTION

Introduction to CO_2 and CH_4 Flux in Tidal Marshes

Tidal salt marshes store and cycle large quantities of carbon, potentially effluxing significant carbon dioxide (CO_2) and methane (CH_4) greenhouse gases to the atmosphere under certain environmental conditions. In the context of global climate change, there is increasing attention on accurately quantifying the amount of CO_2 and CH_4 produced and effluxed by these ecosystems (IPCC 2014). Past research indicated that estuaries contribute CO_2 to the atmosphere, but are not a significant source of CH_4 due to the inhibitory effects of sulfate (SO_4^{2-}) found in seawater (Lovley and Phillips 1987). Additionally, previous research found a strong negative correlation between CH_4 flux and salinity from 0 to 26‰ with near complete cessation of CH_4 flux above 20‰ salinity (Poffenbarger et al. 2011). However, more recent work demonstrated that the presence of seawater at levels higher than 9 ‰ does not necessarily inhibit CH_4 production (Van Der Nat and Middelburg 2000; Weston et al. 2006; Middelburg et al. 2014; Wilson et al. 2015) and instead the CH_4 production in salt marshes depends on the carbon source availability (Holmer and Kristensen 1994), temperature (Avery et al. 2003), and redox conditions (Lovley and Phillips 1987). Thus, the role of tidal marshes in atmospheric CH_4 flux and the magnitude of that flux is unresolved with yearly estimates of 150 ± 221 g m^{-2} s^{-1} (Poffenbarger et al. 2011). In addition, past research has focused predominantly on areas in and around tidal channels, with most studies amalgamating production and flux of greenhouse gases from limited

spatial sampling based on an assumption of homogeneity across estuary marsh. We may be under- or overestimating C fluxes and pools in marshes by neglecting spatial heterogeneity in both production and flux across a tidal salt marsh and within a soil column. Moreover, with uncertain estimates on the current magnitudes of C pools and fluxes, uncertainties in future predictions of changes to C pools and fluxes due to climate and land-use change (i.e. sea level rise, increased storm frequency, urbanization) will be exacerbated.

Literature Review

Previous studies in peatlands and wetlands found that water table depth is a primary indicator of CO_2 and CH_4 production due to the effect of inundation on biogeochemistry, specifically redox conditions (Moore and Dalva 1993; Moore and Roulet 1993; Kelley et al. 1995; Wachinger et al. 2000; Smith et al. 2003). Peatlands and wetlands have similar water table depth variations (0-60 cm) (Mer and Roger 2010) to tidal salt marshes (Wolanski 2007). However, water table elevation and inundation in wetlands vary on a seasonal scale, whereas water table elevation and inundation depth in tidal marshes vary on daily to fortnightly periods as well as seasonally (Wolanski 2007).

Seasonal water table shifts and temperature dependence of microbial activity gives CO_2 and CH_4 production distinct seasonal trends, with high flux during a warm growing season and little to no flux in the winter months, in wetlands. However, water tables in a tidal marsh fluctuate diurnally and can be highly variable across the ecosystem, causing CO_2 and CH_4 production, as well as flux rates, to have both seasonal and diurnal patterns (Chanton et al. 1989; Maher et al. 2015).

Tidal influence is variable across a marsh due to differences in topography and proximity to tidal channels across and ecosystem (Drabsch et al. 1999). Water table variations can range from daily swings in the water table caused by tides (~ 10 cm)**,** to no daily variation in water table (Drabsch et al. 1999; Montalto et al. 2007) depending on the location within a salt marsh. However, even in areas with little to no daily variations, there can be obvious longer scale variations caused by spring-neap tidal dynamics. Differing water table dynamics across an estuary lead to spatial heterogeneity of biogeochemical processes, including CO_2 and CH_4 production, in marshes. Water table and inundation dynamics change porewater and solid-phase chemistry by altering the availability of chemical components (i.e. amount of seawater and carbon), which happens on a different timescale than that of wetlands and peatlands.

Tides can also affect the balance of CO_2 and CH_4 production by impacting microbial activity through replenishment of dissolved organic carbon (DOC) and terminal electron acceptors (TEAs), two necessary components of CO_2 and CH_4 production. Tides consistently deliver sulfate (SO_4^{2-}), a TEA, to the marsh. This potentially stimulates the activity of sulfate-reducing bacteria (SRBs), which compete with methane producing bacteria (methanogens) for carbon substrates, and thus, may result in more CO_2 and less CH_4 production (Weston et al. 2010). A receding tide can also drain portions of the marsh enough to oxygenate the sediments or to allow O_2 to re-oxidize some spent TEAs, and thus replenish the supply of TEAs for microbial respiration (Kelley et al. 1995; Segers 1998; Smith et al. 2003). In the absence of more favorable TEAs, CH_4 is produced by using the CO_2 in the soil column as a TEA by methanogens. In tidal marshes, this is likely to occur in areas that are not routinely

exposed to oxygen with the receding tides, because even a brief period of aerobic conditions, such as an ebbing tidal cycle, may significantly limit CH_4 production (Kelley et al. 1995). Therefore, the current paradigm in tidal marsh systems is that the more energetically favorable TEAs rarely become depleted and conditions are favorable for CO_2 (and not CH_4) production and flux (Poffenbarger et al. 2011). However, methanogenesis and sulfate reduction can occur concurrently in the presence of a large and/or variable DOC source (Mer and Roger 2010), with the less energetically-favorable methanogenesis occurring at a slower rate than sulfate reduction (Grill and Martens 1986; Kuivila et al. 1990; Avery et al. 2003). High tides can bring in a new source of DOC, which is the energy source for microbial activity and is often the rate-limiting component in microbial respiration (Winfrey and Zeikus 1977; Holmer and Kristensen 1999).

Tidal cycles also have implications for sediment-air gas exchange. During periods of inundation, CO_2 and CH_4 produced within the soil column would have limited conduits to escape to the atmosphere through sediment pore spaces, and could become trapped within the soil column, especially if the gases are produced below the rooting depth of the dominant vegetation as aerenchyma can act as a conduit for gases to escape. However, the outgoing tide may also allow trapped gases to escape, a process known as tidal pumping. Tidal patterns for both CH_4 and CO_2 flux have been observed with eddy covariance towers and within the tidal streams as dissolved gases (Beck et al. 2008; Grunwald et al. 2009; Tong et al. 2013; Call et al. 2015). In the aforementioned studies, both dissolved CH_4 and CO_2 concentrations had an inverse relationship with tidal amplitude, indicating a flushing effect with low tide. However, these studies are limited to dissolved CO_2 and CH_4 in the tidal channels and do not

quantify gas production with depth and fluxes directly from the soils over spatial and long-term temporal gradients. We reason that there is a potential for CO_2 and CH_4 gases to flux directly from sediments in a marsh during tidal cycles, or tidal pumping events, because the absence of inundation during low tide can allow for gases trapped deeper in the sediment profile to escape directly to the atmosphere. This type of gas flux is not accounted for in studies that only quantify dissolved gases from tidal channels. Additionally, spatial heterogeneity of hydrological regimes can cause low tide flux to vary across a tidal salt marsh.

Research Goals and Objectives

In this study, we aim to understand how biogeochemical and water table elevation spatial gradients affect CH_4 and CO_2 production and flux in a salt marsh. We evaluated the temporal and spatial heterogeneity of biogeochemical cycling of redox-sensitive parameters and CO_2 and CH_4 production and flux in a single tidally influenced salt marsh. We hypothesize that 1) changes in sediment chemistry due to varying hydrological regimes will affect production and flux of CO_2 and CH_4 and that this will vary spatially and temporally due to differences in water table fluctuations and thus sediment biogeochemistry across a marsh; 2) areas with higher variability in water table depth will have a greater rate of flux than those with less variation in water table depth; and 3) areas with low water table fluctuations will exhibit seasonal changes in CO_2 and CH_4 fluxes, whereas areas with high water table fluctuations will have more variation in CO_2 and CH_4 fluxes over shorter time scales. To test these, two subsites with different tidal influence and hydrological regimes were monitored over a one-year period for changes in pore-water chemistry at discrete depths to -90 cm as well as CO_2 and CH_4 gas flux to the atmosphere at both subsites. In addition, we more

intensely monitored gas production with depth to -70 cm and hydrological dynamics at these subsites by monitoring gas production at depth and water table elevation over the course of one summer month.

Chapter 2

MATERIALS AND METHODS

Study Site

This study took place in the St. Jones Reserve, a coastal estuary outside of Dover, Delaware (Fig. 1). The St. Jones is part of the National Estuarine Research Reserve System (NERRS) and is managed by the Delaware Department of Natural Resources and Environmental Control (DNREC). The St. Jones Reserve is 15.2 km^2 with an 8.8 km stretch of medium salinity tidal river (~8-25 ‰). This river is a tributary of the St. Jones River that drains agricultural land but also experiences tidal inundation from the Delaware Bay, as the St. Jones River is a tributary of the Delaware Bay. This region experiences a temperate climate with average temperature ranging from 0°C in the winter to 25 °C in the summer with a yearly average temperature of 15°C, and receives about 100 cm annual precipitation (Fig 2a). High tides occur twice daily with amplitudes ranging from ~1 m to ~1.5 m during neap and spring tides, respectively (Fig 2b).

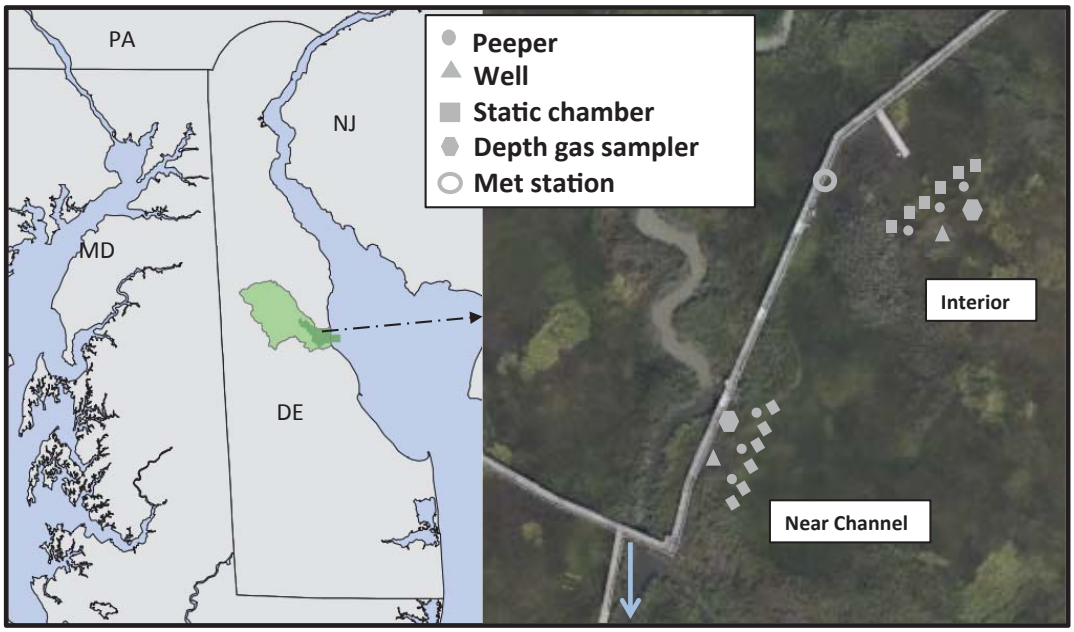

Figure 1 Map of Delaware and surrounding states with the St. Jones River watershed highlighted in light green (left panel). An aerial view of the sampling type and location at the DNERR St. Jones Reserve (right panel). The arrow represents the flow of tidal channel during low tide.

The reserve has continuous monitoring of meteorological data managed by the Delaware Environmental Observation System (DEOS), and water quality data that includes salinity, water temperature, conductivity, pH, turbidity, and dissolved oxygen managed by DNREC. There is a tidal gauge monitoring system at the confluence of Leipsic River and the Delaware Bay managed by the NOAA, which is about 3 km north of the confluence of the St. Jones River and the Delaware Bay.

To capture spatial heterogeneity at the site, we identified two biogeochemically distinct subsites: one proximal to the tidal channel (hereafter referred to as “near channel”), and the other approximately 70 m from the channel (hereafter referred to as “interior”) (Fig. 1). *Spartina cynosuriodes* L. is the dominant vegetation at the near channel subsite and *S. alterniflora* L. is the dominant vegetation at the interior subsite.

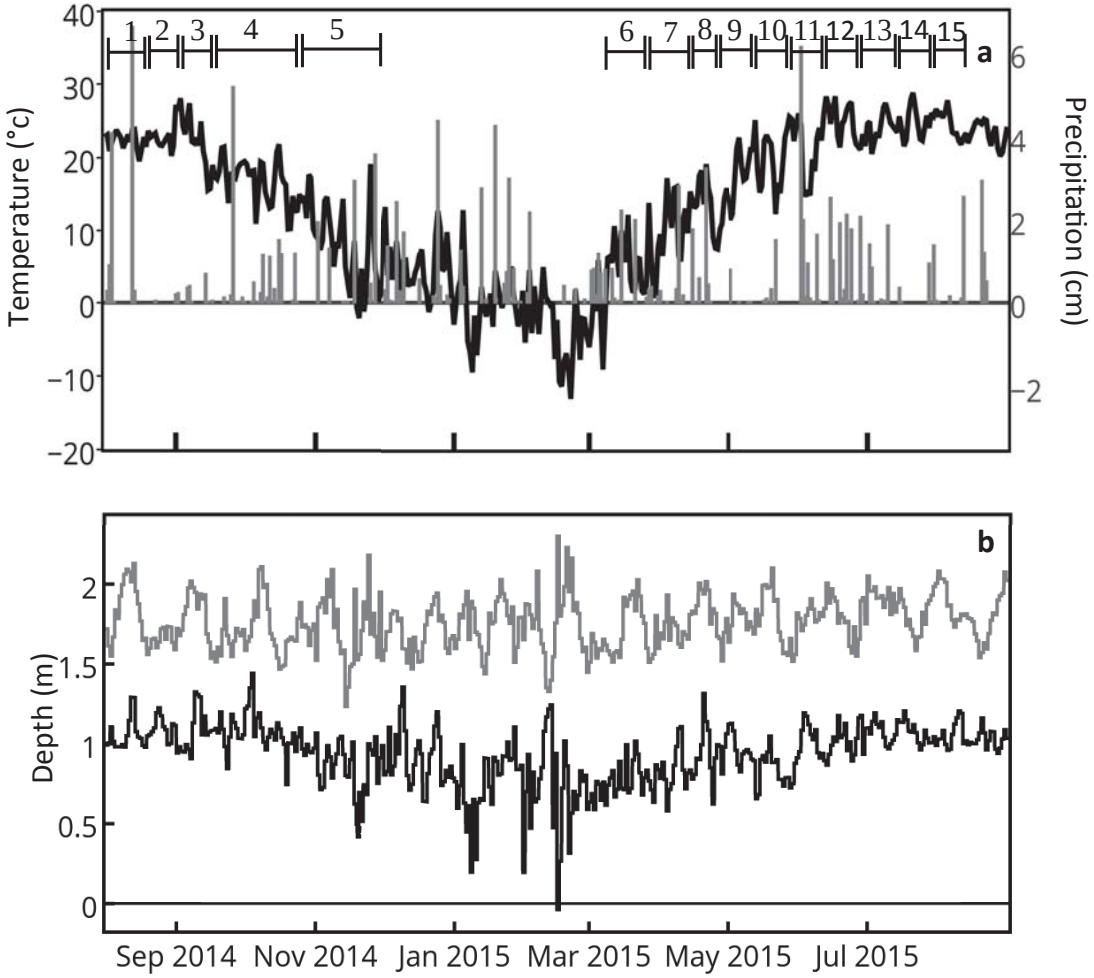

Figure 2 (a) Average daily temperature (black) and precipitation (grey) at the St. Jones Reserve with the 15 sampling periods labeled 1-15 and (b) average daily mean (black) daily difference between high and low tide (grey) at the confluence of the Liepsic River and the Delaware Bay, located approximately 3.2 km north of the St Jones Reserve.

Porewater Sampling

Porewater samples were collected at discrete depths at each subsite using passive porewater samplers (i.e., peepers) in triplicate (i.e. peeper nests) modified from LaForce et al., (2000). A PVC pipe (8.5 inch diameter, 60 inch length) housed 9-10 cells, which hold the peepers. Peepers consisted of 13 mL polypropylene tubes fitted with a plastic cap, which contains a 0.20 micron filter and initially filled with 18 MΩ water. The near channel subsite had peepers at 9 depths (0, -3, -12, -25, -40, -50, -65, -75, -90 cm) and the interior subsite had peepers at 10 depths (0, -3, -12, -25, -35, -45, -55, -65, -75, -90 cm) relative to the soil surface. Each depth corresponded with a soil horizon with at least two peepers per horizon (Fig 3a and b). The peepers were allowed to equilibrate for at least 10 days (LaForce et al. 2000). After equilibration, the peeper cells were removed from the housing and immediately replaced with fresh peeper cells. When removed from the housing, the peeper cells were immediately placed inside a gas impermeable container with oxygen scrubbers and sealed. The samples were placed on ice and were analyzed or preserved within two hours. Sampling occurred approximately every two weeks between 8/13/14 and 8/24/15, with a three-month hiatus between 12/15/14 to 3/27/15 when air temperatures were below freezing.

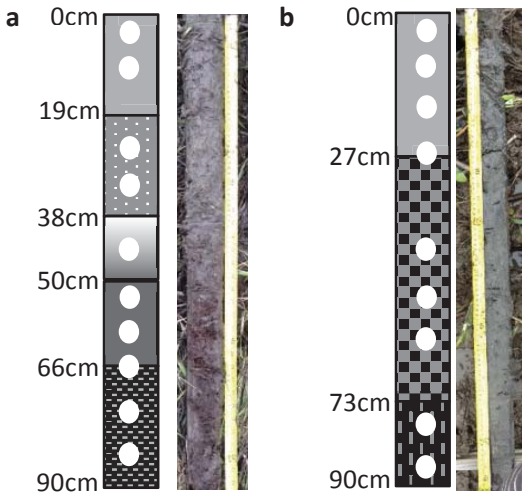

Figure 3 A schematic of the horizonation of both the near channel (a) and the interior (b) on the left with a photograph of the sediment core on the right. White dots indicate peeper cell locations.

Each sample was aliquoted into different tubes for various analyses by using a syringe fitted with a needle to pierce the peeper cell membrane and withdraw the 13 mL of equilibrated water sample. For redox and pH measurements, 2 mL sample was placed into a polypropylene tube and measured with calibrated probes within 5 minutes of removing the samples from the sealed, gas-impermeable container. Concurrently, 1 mL of sample was added to a mid range sulfide determining reagent (8 g N N-dimethyl-*p*-phenylenediamine and 8 g $FeCl_3$ in a 50% HCl solution). The solution was allowed to sit for at least 20 minutes and was then measured at 667 nm in accordance with the Cline method within 24 hours (Cline 1969). Samples that were out of range were diluted further with deoxygenated water until it was within the range of the spectrophotometer (Reese et al. 2011). Additionally, 0.5 mL of sample was added to 4.45 mL of ferrozine reagent (1 g L^{-1} of 3- (2-Pyridyl)-5,6-diphenyl-1,2,4-triazine-40,400-disulfonic acid sodium salt in 50mM HEPES buffer) and 0.05 mL of 18 MΩ water and measured at 562 nm within 24 hours (Stookey 1970).

Elemental analysis of iron using microwave plasma- atomic emission spectrometry (MP-AES, HP 4100) was conducted on 5 mL of sample after 1:1 dilution and acidification with 2% trace metal grade nitric acid. At least 1 mL and 3 mL of samples were frozen in separate tubes for ion chromatography (IC) and dissolved organic carbon (DOC), respectively. DOC samples were diluted after thawing in a 1:5 ratio with 18 MΩ water and analyzed (Elementar Vario-TOC cube), and the IC samples were diluted in a 1:3 ratio after thawing. Nitrate, sulfate and phosphate were separated on an AS18 column equipped with an AG18 guard column in gradient elution mode with 20 mM KOH eluent from 0 to 13.5 min and a ramp to 45 mM from 13.5 to 16 minutes and analyzed by electrical conductivity detection (Dionex DX-500). Conductivity was also measured on select samples (Thermofisher Orion STAR A322).

Soil Extractions

A 90 cm soil core was taken at each subsite in June 2014. The soil cores were sectioned into three sections (0-27, 27-73, 73+ cm) for the near channel and 5 sections (0-19, 19-38, 38-50, 50-66, 66+ cm) for the interior subsite's corresponding to soil horizon locations (Fig. 3a and b).

Ammonium oxalate (AO) extractions were performed in accordance with McKeague and Day (1966). AO extractions were performed by sieving dried, crushed and homogenized sections of the cores to 0.15 mm. Ammonium oxalate (30 mL, 0.2M) was added to soil samples (0.5g) and let sit in the solution in the dark for two hours. The solution was then centrifuged, decanted, filtered, and acidified with 2% trace metal grade nitric acid (McKeague and Day 1966).

Citrate-bicarbonate-dithionite (CBD) extractions were performed in accordance with Mehra and Jackson (1958). CBD extractions were performed using the same dried, crushed and homogenized sections of the cores. The soil was sieved to 0.053 mm. Sodium citrate (1mL, 0.30M) and sodium bicarbonate (1mL) were added to 1g of soil. The mixture was brought to a temperature of 80 ˚C, when sodium dithionite (0.4 g) was added in two half-doses and reacted for 10 minutes. A saturated sodium chloride solution (2 mL) was then added. The samples were then centrifuged, decanted, filtered and acidified with trace metal grade nitric acid (Mehra 1958). All extracts were analyzed for total elements using ICP-OES (Thermo Elemental Intrepid II XSP Duo View).

Gas Sampling

Surface Sampling

Fluxes of CH_4 and CO_2 were measured using a Los Gatos Research Portable Gas Analyzer (LGR-PGA) using the static flux chamber method. Twelve PVC rings were inserted into the sediment at the near channel and interior subsites, 6 per subsite, and arranged such that they were adjacent to the peeper nests and 180 degrees away from foot traffic in the marsh (Fig. 1). No samples were taken until at least 2 weeks after the placement of the rings to allow the area around the rings to return to a previous, undisturbed state. The rings remained in the surface sediments throughout the 1-year sampling duration.

During sampling, a PVC flux chamber was placed onto the fixed ring, and the chamber was connected to the LGR-PGA with gas-tight tubing for 3 minutes to establish a rate. Flux samples were taken every other week between June 2014 and

September 2015 except for a hiatus during the winter months (12/15/14 to 3/27/15) and the initial spring thaw in March 2015 during which samples were taken weekly for 4 weeks. Flux measurements always occurred within an hour of low tide. Surface soil temperature was measured at the time of flux using an infrared thermometer (Arctic Star AR550). Flux was calculated by using the slope of the flux observed, after subtracting the first 30 seconds of flux, with the following equation:

$$Gas\ Flux = \frac{\delta c}{\delta t} * \frac{V}{S} * \frac{P}{RT} \quad (1)$$

where $\frac{\delta c}{\delta t}$ is the mole fraction of the gas in μmol mol^{-1} over time (s), V is the volume of the flux chamber (0.0011m3), S is the surface area enclosed by the chamber (0.0081m2), P is the atmospheric pressure (assumed to be 101.325 kPa), R is the universal gas constant (8.3×10−3 m3 kPa mol−1 K−1), and T is the soil temperature at time of fluxing (K). The change in concentration of gas over time, or $\frac{\delta c}{\delta t}$, was calculated by fitting a linear regression for CH_4 and CO_2 for each measurement. Only values where $r_2 > 0.85$ and $p < 0.05$ were used in flux calculations. Erroneous fluxes where signs of poor measurement were observed (i.e., an initial spike in $\frac{\delta c}{\delta t}$ followed by a negative slope was indicative of sediment disturbance) were not included in calculations. All flux values from the interior or from the near channel subsites were averaged together (n=6) for each sampling date.

Depth Sampling

In order to address spatial heterogeneity of gas production vertically in the sediments, depth profiles of CH_4 and CO_2 concentrations were measured from July 2015 to August 2015 using a modified passive gas sampling device (Jacinthe and Groffman 2001). Gas-permeable silicone tubes (12.7mm inner diameter and 3.175

mm-thick) were placed inside a 2.34 cm x 91.4 cm polypropylene sheet with rectangular through holes cut out at 4 discrete depths depending on subsite horizonation (near channel: -17.5, -30, -50, -68 cm and interior: -15.5, -40, -56, and -70 cm relative to the soil surface) (Fig 4). Each silicone tube was 23.5 cm long and was attached to gas-tight vinyl tubing on each end by a corrosion resistant L-joint. Each joint was made gas- and water-tight with silicone sealant and allowed to dry and harden prior to deployment at the field site. Barbed three-way valves were attached on one end of each of the vinyl tubes and a barbed two-way valve was attached to the other vinyl tube end. Gas-tight Teflon tubing was attached to one of the barbs on the three-way valve for ready coupling to the LGR-PGA with push-to-connect fittings, and Teflon tubing was also attached to the two-way valve barbed for ready coupling to a gas-tight bladder bag of N_2. The apparati were buried at each subsite (Fig. 1) by hammering the plastic frame into the soil with a rubber mallet to limit disruption oxygenation of the soil. The apparati were allowed to equilibrate with the sediments for two weeks before initial measurements were made. During sampling, the LGR-PGA and N_2 bladder bag were connected to opposite ends, and the valves were opened to allow accumulated gas to flow into the LGR-PGA for measurement. Concentrations of CH_4 and CO_2 were measured until a sharp drop in concentration was observed, indicating the N_2 had cleared the chamber of CH_4 and CO_2. After sampling, the valves were closed to ensure both an air- and water-tight system. This was repeated at each depth at each subsite during weekly sampling from 7/13/15-8/12/15. The LGR's high limit of detection was 829 µM (20,000ppm) for both gases, and values over this limit were recorded as >829 µM.

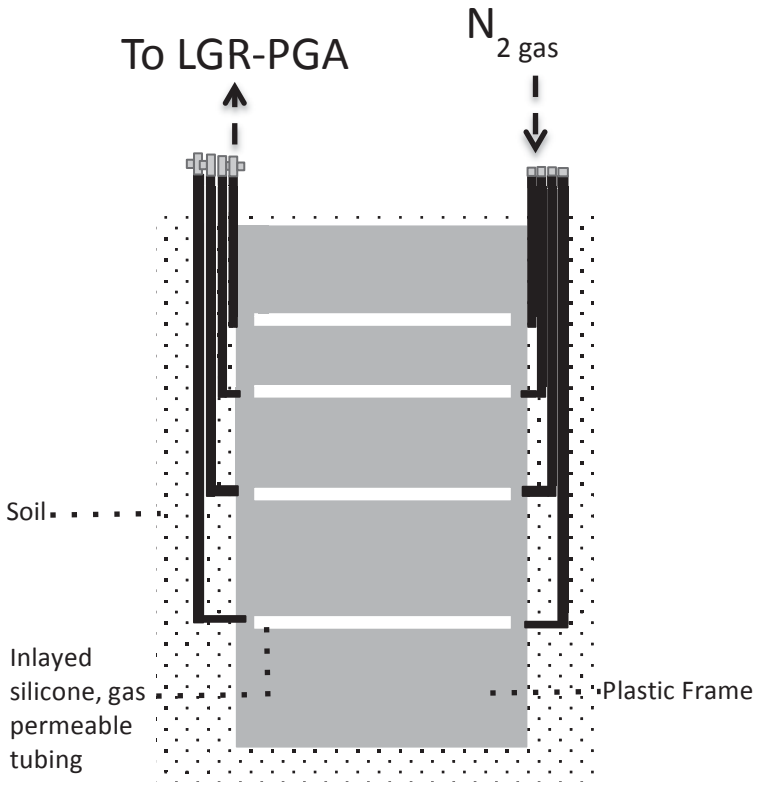

Figure 4 A schematic of the depth gas-sampling device buried in the sediments.

Hydrological Sampling

A 90 cm-deep well was placed within 3 m of each peeper nest at each subsite (Fig. 1). Each well consisted of a slotted PVC pipe that contained a conductivity, temperature and depth (CTD) sensor (Aqua TROLL 200 Data Logger). A pressure transducer (Baro-Diver) was installed at the near channel subsite to record the

atmospheric pressure, and these data were used to calculate water table height for both sites according to the following equation:

$$H = \frac{P_{obs} - P_{Atm}}{\rho g} \quad (2)$$

where P_{obs} is the pressure recorded by the CTD, P_{atm} is the atmospheric pressure, ρ is the water density and g is gravity. The height was corrected to establish a 0 value at the soil surface by measuring the water table depth manually at both sites on 9/22/15. Water table depths at both sites were measured between 7/8/2015 and 10/6/2015 and covered the range of depth gas sampling.

Spring-neap tidal times were determined by using NOAA astronomical data. Where the spring tide time was defined as occurring at full and new moons and neap tides occurring during first and third quarter moons.

Statistical Analysis

Biogeochemical parameters over time were compared between the two sites by averaging all depths per sampling time and using two-tailed *t*-test where unequal variance is assumed. Standard error was calculated for each parameter where n=3 for biogeochemical parameters and n=6 for surface gas flux. Variance was calculated across all depths over the entire sampling period for redox values at both sites.

Chapter 3

RESULTS

Porewater

Spatial heterogeneity in porewater chemical signatures was clearly apparent laterally between the near channel and interior subsites, as well as vertically within each subsite (Fig. 5).

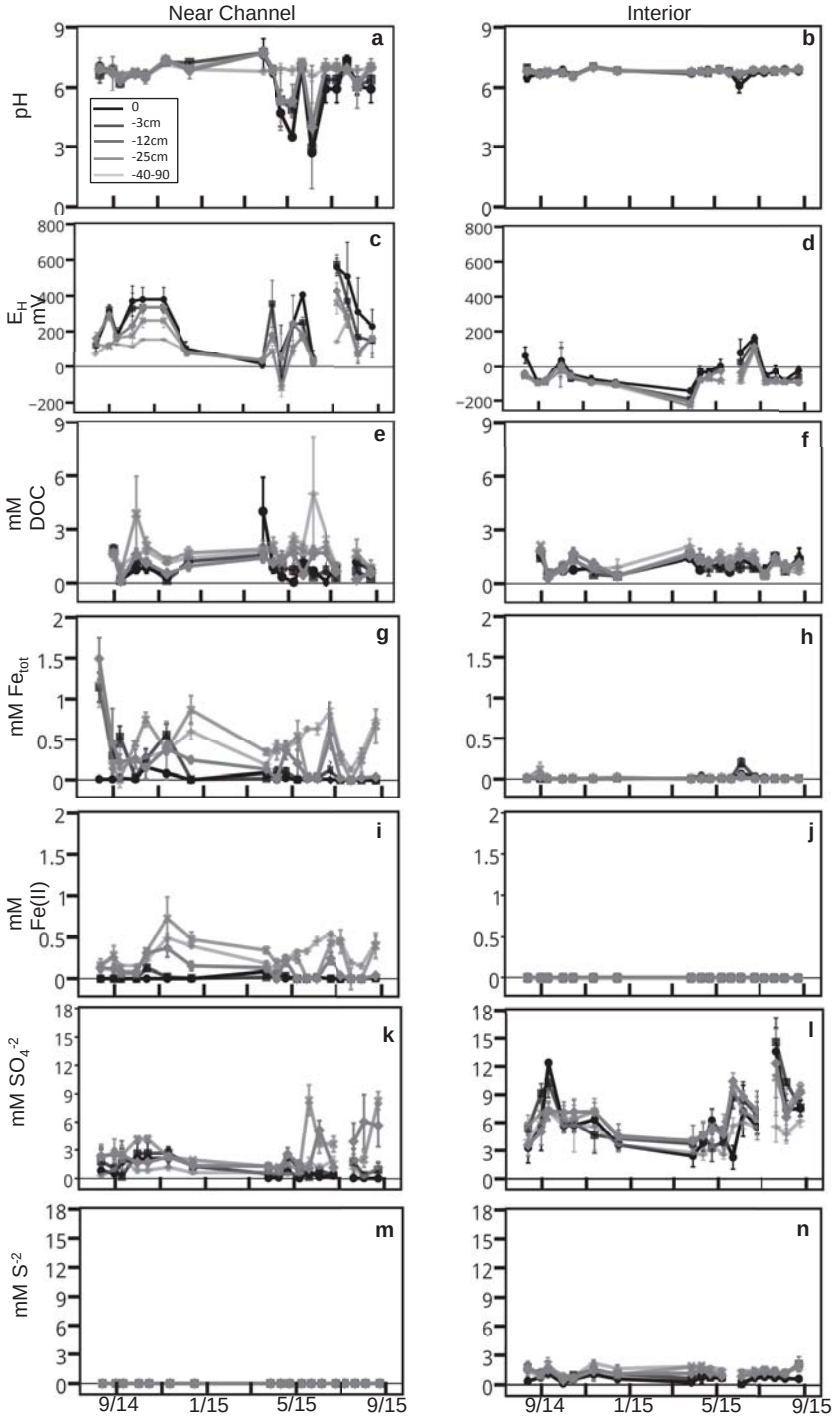

Figure 5 Average (±SE, *n*=3) porewater pH (a, b), redox (c, d), DOC (e, f), total Fe (g, h), Fe (II) (i, j), SO_4^{2-} (k, l) and S^{2-} (m, n) for both near channel (a, c, e, g, i, k, m) and interior (b, d, f, h, j, l, n) subsites.

pH

The near channel subsite had more variable pH both with depth and over time compared to the interior subsite (5 a and b). The interior subsite was consistently between a pH of 6 and 7, whereas the near channel subsite had variation near the surface, ranging from 3.5 to 7.6.

Redox

At both the near channel and interior subsites, seasonal trends in porewater redox were observed. Redox values across all depths and at both sites decreased during winter plant senescence and then increased during the spring and summer growing season. While both subsites showed seasonal variation at all depths, they had different redox values and depth variation.

The interior subsite had significantly lower average redox values compared to the near channel subsite over time ($p < 0.05$) (Fig. 5c and d). Redox values for the interior subsite were consistently low and nearly always negative, ranging -200 to 200 mV with depth. In contrast, redox at the near channel subsite tended to decrease with depth, with the highest redox value of 575 mV recorded at the sediment-air interface and the lowest of -118 recorded at depth. This trend was more prevalent during the growing season (May-September). Redox values decreased with depth during the growing season, but were more uniform during late fall and winter sampling. The near channel subsite had an order of magnitude higher variance in redox with depth compared to the interior subsite (18581 and 4763, respectively), with surface

porewater Redox values ranging widely from 0 to 600 mV, and deeper redox values more narrowly ranged from ca. 0 to 300 mV.

DOC

The near channel subsite has more variable dissolved organic carbon both with depth and over time compared to the interior subsite (Fig. 6e and f). Concentrations ranged 0 to 4.0μM at the near channel subsite. In contrast, the interior subsite exhibited little variation in DOC concentration with both depth and time with values ranging 0 to 1.7 μM.

Fe and S

The near channel and interior subsites differed greatly in the magnitude and speciation of iron and sulfate compounds in porewater (Fig. 5g-n). Total iron at the near channel subsite was as high as 1.5 mM and increased with depth (Fig. 5g) whereas total iron at the interior subsite was rarely detectable (Fig. 5h) despite similar amounts of CBD- and AAO-extractable iron (Table 1). Similar trends were observed with iron (II), with concentrations up to 1.0 mM at the near channel subsite and non-detectable at the interior subsite (Fig. 5i and j). At the near channel subsite, total iron concentrations equaled iron (II) concentrations at depth indicating that all the iron present was reduced at depth below -12 cm.

In contrast to iron, concentrations of sulfate compounds at the interior subsite were higher than at the near channel subsite. Sulfate concentrations ranged from non-detectable to 9.0 mM at the near channel subsite, whereas at the interior subsite they ranged 3.0 to 18 mM (Fig. 5k, l). Sulfate concentrations varied with depth in an inconsistent manner; however, sulfide concentrations were non-detectable at the near

channel subsite (Fig. 5m) but were detectable at all depths at the interior subsite ranging 0.10 to 2.2 mM and tending to increase with depth (Fig. 5n).

Table 1 Citrate-bicarbonate-dithionate (CBD) extractable Fe and acid ammonium oxalate (AAO) extractable Fe in the near channel and interior subsites.

	Depth (cm)	CBD-extractable Fe (mmol kg^{-1})	AAO-extractable Fe (mmol kg^{-1})
Near channel	**0-27**	13.8	152
	27-73	11.1	196
	73+	10.1	298
Interior	**0-19**	10.5	212
	19-38	9.60	228
	38-50	14.5	201
	50-66	13.9	110
	66+	5.20	44.4

CO_2 and CH_4

Surface Flux

Methane fluxes were as high as 0.87 and 1.4 μM m^{-2} s^{-1} at the near channel and interior subsite, respectively, during the two growing seasons measured, and CO_2 fluxes were as high as 17 and 12 μM m^{-2} s^{-1} at the near channel and interior subsite, respectively. The daily average CO_2 flux values (207 mmol m^{-2} d^{-1} and 462 mmol m^{-2} d^{-1} at the interior and near channel respectively) are comparable to literature values for tidal salt marshes (12 - 660 mmol m^{-2} d^{-1}), whereas the average CH_4 flux values (11.8 and 9.4 mmol m^{-2} d^{-1} for the interior and near channel subsites, respectively) are larger than previously reported values for similar salt marshes (0 - 7.1 mmol m^{-2} d^{-1})(Abril and Borges 2004).

Surface fluxes of both CH_4 and CO_2 have a distinct seasonal trend at both sites (Fig. 6a and b). At both sites, the highest CO_2 fluxes occurred on the same day (8/22/14) whereas the highest CH_4 fluxes occurred on different days for the near channel (7/29/15) and interior (8/22/14) subsites. During plant senescence, fluxes of both CH_4 and CO_2 declined and were near zero in the winter (Fig. 6). Both sites exhibit similar flux patterns and tended to increase and decrease in unison for both gases, yet CO_2 flux was consistently higher for the near channel subsite compared to the interior subsite (Fig. 6b). Methane spiked in July-September at both subsites for both years, yet the magnitude differed for each year with interior having a higher CH_4 spike than near channel in 2014, and the converse was observed in 2015 (Fig. 6a).

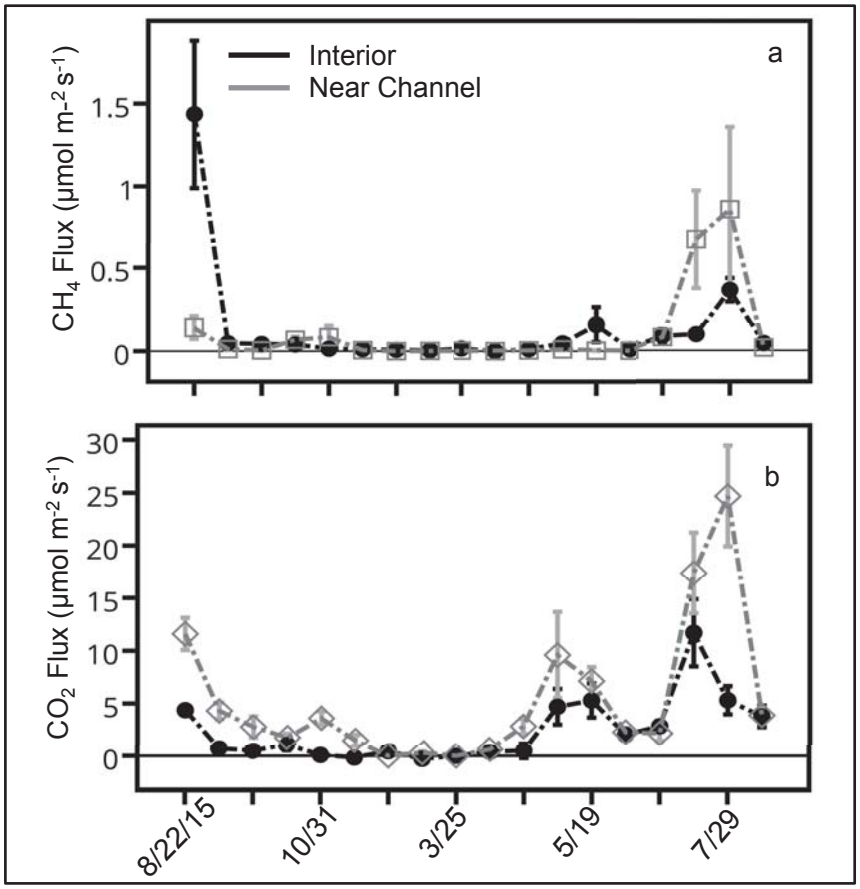

Figure 6 Average CH_4 (a) and CO_2 (b) gas flux (±SE, *n*=6) from interior and near channel subsites.

Hydrology

We sought to examine production of CO_2 and CH_4 at each subsite with depth due to wide variations in water table elevations and periods of land surface inundation at each subsite (Fig. 7). The near-channel and interior subsites had significantly different water table depths ($p < 0.05$) over the time period of 8 July 2015- 6 October 2015. The interior subsite exhibited daily tidal variations in water table depth, whereas the near channel subsite varied primarily on longer time scales associated with the spring-neap cycle (Fig. 7a). The water table elevation at the interior subsite normally

fluctuated from ca. -5 cm to the sediment surface. However, there was occasional standing water present and the interior subsite had water level values up to +20 cm and as high as 60 cm during a storm surge. Fluctuations at the near channel subsite were greater and ranged from -25 cm to the water surface, with standing water levels reaching +10 cm and occasionally as high as +40 cm during a storm surge (Fig. 7a). In the period of depth-gas sampling, the interior subsite was consistently inundated whereas the near channel subsite exhibited cyclical variation of the water table depth evident with a sharp increase followed by a prolonged, multiple-day drop off in water table elevation (Fig. 7b). This variation in water table depths at the near channel subsite occurs with the spring-neap tidal cycle where spring tides coincides with higher water table elevations and neap tides cycle coincides with lower water table elevations.

CO_2 and CH_4 Production with Depth

Depth profiles of CO_2 and CH_4 concentrations taken on 5 different days over a spring/neap tidal cycle show an apparent build up of both CH_4 and CO_2 in the subsurface at both subsites, but the interior subsite typically had higher CH_4 and CO_2 concentrations at depth (ca. > -30 cm) compared to the near channel subsite (Table 2).

At the interior subsite, CH_4 concentrations were highly variable at the uppermost sampling depth ranging from 0.800 to 661 μM across the sampling period (Table 2). This was also true for CO_2 concentrations with values ranging from 17.9 to above 829 μM. However, both CO_2 and CH_4 concentrations increased sharply with depth. At -40 cm, CO_2 concentrations exceeded the LGR-PGA detection range of 829 μM. CH_4 also increased with depth, but not always as high as CO_2 concentrations (Table 2).

At the near channel subsite, the uppermost sampling depth had CO_2 concentrations ranging from 209 to > 892μM. CO_2 concentration increased with depth and reached detection range and was >892 μM at -30 cm. The near channel subsite had less CH_4 present in the upper first 30 cm of the soil column than the interior subsite. While the interior subsite did exhibit an increase in CH_4 concentrations with depth, the concentrations present were an order of magnitude smaller than the interior subsite. Additionally, concentrations only went beyond the detection range on three occasions and were deeper in the soil column.

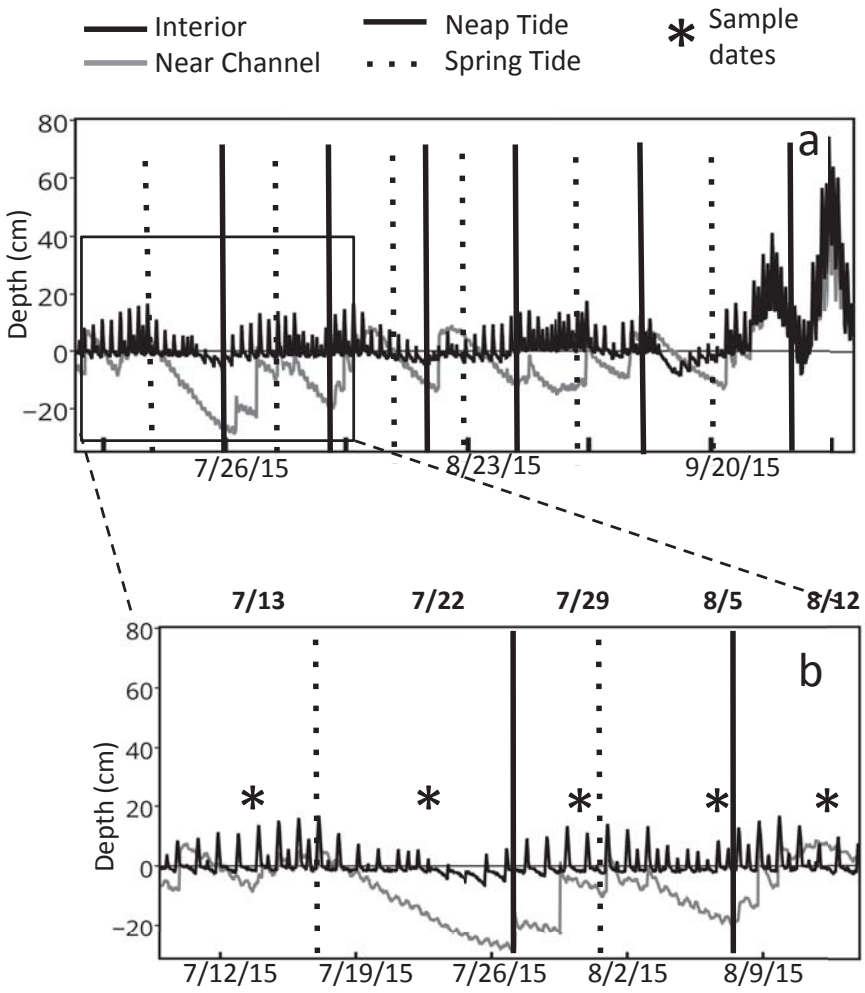

Figure 7 Water table elevations at the interior (black) and near channel (grey) sub-sites during the summer-fall 2015 sampling period with spring-neap tides overlaid (black dotted and solid lines respectively)(a) and a zoomed in plot of (a) where asterisks and the corresponding dates above indicate the sampling days for depth gas sampling (b) and reported in Table 2.

Table 2 CH_4 and CO_2 concentrations (μM) over a month sampling period using the depth gas samplers at both sites.

		7/13		7/22		7/29		8/5		8/12	
	Depth (cm)	CH_4	CO_2	CH_4	CO_2	CH_4	CO_2	CH_4	CO_2	CH_4	CO_2
Near Channel	**-17.5**	4.20	209	7.80	517	1.6	371	2.10	233	22.1	*>892*
	-30	55.2	>892	40.2	>892	19.7	*>892*	25.0	*>892*	93.3	*>892*
	-50	79.8	>892	68.1	175	*>892*	*>892*	602.9	*>892*	511.5	*>892*
	-68	239	>892	*>892*	>892	*>892*	*>892*	588.9	*>892*	313.2	*>892*
Interior	**-15.5**	660	*>892*	0.8	17.9	0.80	19.0	---	---	254	196
	-40	267	*>892*	655	*>892*	615.8	*>892*	---	---	321	*>892*
	-56	510	*>892*	*>892*	*>892*	665.1	*>892*	---	---	*>892*	*>892*
	-70	270	*>892*	652	*>892*	*>892*	*>892*	---	---	*>892*	*>892*

Chapter 4

DISCUSSION

Spatial Heterogeneity in The Tidal Marsh

Spatial Heterogeneity of CH_4 and CO_2 Flux

Our data shows that water table depth variability results in both a lateral (across the marsh) and vertical (with depth) heterogeneity in biogeochemical processes that, in turn, causes a spatial heterogeneity of CO_2 and CH_4 production and flux. The subsite proximal to the tidal channel, where water table fluctuations were larger, had variable but relatively high redox values due to reoxygenation of sediments. This resulted in higher CO_2 (0-25 μmol m^{-2} s^{-1}) and typically lower CH_4 (0-1.0 μmol m^{-2} s^{-1}) flux compared to the subsite farther from the tidal channel where water table fluctuations were smaller. Due to small water table elevation fluctuations, the interior subsite was frequently inundated, which resulted in few opportunities for reoxygenation and consequently lower redox values and lower CO_2 (0-12 μMol m^{-2} s^{-1}) and slightly higher CH_4 (0-1.4 μMol m^{-2} s^{-1}) flux. The spatial heterogeneity of inundation due to hydrologic factors likely led to differences in dominant anaerobic (iron(III) reduction vs. sulfate reduction) and aerobic soil respiration processes at the two subsites, which in turn affects the production and flux of CO_2 and CH_4 to the atmosphere. Denitrification is another spatially variant anaerobic respiration process that occurs in a salt marsh, but is beyond the scope of this study.

The variability in the water table elevation caused distinct differences in the redox profile at the two subsites. The interior subsite, while more tidally influenced, was almost always inundated and had uniformly low redox values both with depth and across the sampling time period (Fig. 5d) due to the inundation. While there was greater daily variation in water elevations than seen at the near channel subsite, this variation was primarily above land surface, only affecting the top 3 centimeters of the water soil column at the interior subsite (Fig. 7a). The high water table elevation and frequent inundation inhibited introduction of oxygen from the surface relative to the near channel subsite. The consistent elevation of the water table elevation (plus occasional inundation) allowed the soil column to become more chemically reduced (Wolanski 2007). Hydrologic and chemical data suggests that the greater daily tidal influence at the interior subsite continually supplied sulfate that was used as a TEA during anaerobic respiration (Fig. 5n). In contrast, the near channel subsite had less daily tidal fluctuation in the water table, but a significant amount of vertical variation over longer time periods from the spring-neap cycle that resulted in periods of falling water table elevation (up to 30 cm depth) (Fig. 7a). This hydrologic process influenced the sediment biogeochemistry such that redox profiles showed patterns of oxic conditions near the surface and less oxic conditions with depth (Fig. 5c). The near channel subsite was close to a brackish tidal channel, which can dilute the high sulfate concentrations present in the seawater brought in by the tides, resulting in lower average sulfate concentrations compared to the interior subsite. While there was sulfate present at the near channel subsite in the porewater, there was no sulfide, which might indicate that there was limited sulfate reduction occurring at this subsite.

Instead, soluble iron was present, which is a more energetically favorable TEA. Microbes that use iron as a TEA have faster reduction rates and preferential DOC consumption than sulfate reducing bacteria (SRBs) (Senior et al. 1982). It is possible for sulfate and iron reduction to have occurred simultaneously, especially in areas where there is limited reducible iron left in the porewater and DOC present (Postma and Jakobsen 1996).

While the geochemistry gives us clues to the dominant microbial processes occurring at each subsite, we cannot rule out iron reduction at the interior subsite, or SO_4^{2-} reduction at the near channel subsite with our data. The sulfide produced might be involved in cryptic cycling, by forming pyrite (FeS_2) with the iron (II) present in the porewater (Howarth et al. 1984; Morse et al. 1987). To fully understand the sulfate and iron dynamics at the tidal marsh, an in-depth investigation into the active microbial community is warranted (Reese et al. 2014). Nevertheless, our data reveal that water table induced differences in dominant sediment biogeochemistry influenced the fluxes of CO_2 and CH_4 at each subsite of the marsh.

The near channel subsite had higher redox potentials than the interior subsite and thus likely had more energetically-favorable microbial processes, like iron (III) reduction and aerobic respiration, dominating in the sediments, resulting in higher CO_2 fluxes compared to the interior subsite. With a lower redox potential, the less-energetically favorable sulfate reduction occurred at the interior subsite and resulted in lower CO_2 flux, but higher CH_4 flux. It is known that iron reduction and CH_4 production do not occur simultaneously as readily as sulfate reduction and CH_4 production (Lovley and Phillips 1987), which supports our observations. For CH_4 to be produced simultaneously with more favorable TEAs, a large carbon source (i.e.

DOC) needs to be present. With a large carbon source, less favorable reactions can occur slowly in microsites (Holmer and Kristensen 1994; van der Nat and Middelburg 1998). Methanogens can cluster around substrates they can easily utilize, like acetate, and thus thrive locally surrounded by SRB (Teh and Silver 2006).

We observed more variable DOC concentrations in the near channel subsite than in the interior subsite. The more variable water table level may account for this variation. Areas with more water table elevation variation have higher variation in DOC due to the import and export mechanisms of the tidal cycle (Fagherazzi et al. 2013). Even though the near channel subsite has less daily variation, the water table at this subsite is lower on average. Therefore there is more of the soil column for water to infiltrate when inundation events occur due to the tide, bringing in new DOC. Areas with the most tidal variation that are well mixed will also have DOC variation (Allen et al. 1980; Abril et al. 2002). DOC can also be present in the tidal channel (Bauer and Bianchi 2011); areas closer to the tidal channel have the potential to receive an influx of DOC. The water table minimum was lower at the near channel subsite, which would allow for DOC to be flushed out of a larger portion of the soil column resulting in more variability in DOC concentrations vertically. Additionally, microbially-mediated carbon mineralization could occur more readily in the upper layers of the soil column due to temperature and light constraints (Alperin et al. 1994). All these factors can lead to more variable DOC concentrations closer to the surface, with the most variation occurring where there are large swings in water table elevation.

Spatial Heterogeneity of CH_4 and CO_2 Gas Concentrations at Depth

In addition to lateral gradients in C gas fluxes between subsites, our study revealed a large pool of stored CO_2 and CH_4 gases with depth > -25 cm that differs in magnitude between each subsite. These concentrations are dependent on both the redox state and on the residence time or the rate of release of gases from the sediments. Measurements over one summer month revealed that CH_4 concentrations ranged 1.6 - >829 μM and 0.8 - >829 μM, and CO_2 concentrations ranged 209 - >829 μM and 17.9 - >829 μM at the near channel and interior subsites, respectively (Table 1). The CH_4 values observed were consistent with literature values for tidal marshes (0-900μM) (Bartlett et al. 1985; Bartlett et al. 1987; Kelley et al. 1995) . However, the aforementioned studies primarily investigated dissolved concentrations with depth in and along a tidal channel. Bartlett et al., 1987 included a CH_4 concentration depth profile at an interior subsite. However the reported CH_4 values (ca. 0-100 μM) were lower than the values observed at the interior subsite. Therefore there is a possibility greater potential for CH_4 efflux from interior sites that has not previously been reported in literature. CO_2 values were not comparable solely due to the fact that the detector was consistently saturated with depth. However, literature values do support dissolved CO_2 concentrations above 829 μM with lower concentrations near the surface at both types of sites.

The uniformity in CH_4 concentrations at the interior subsite can be attributed to the high water table level and inundation extent, which is more favorable for CH_4 production and storage (Table 2). The near channel subsite experienced more variation in CH_4 concentrations with depth. The variation in CH_4 and CO_2 gas concentrations close to the surface at the near channel subsite can be attributed to spring-neap tidal cycles, which causes less frequent inundation than the interior subsite. While redox

and TEA conditions at the near channel subsite were not optimal for CH_4 production, CH_4 was present at all depths and abundant deeper in the soil profile. At the interior subsite, the low redox potential, high DOC concentration and high water table elevation were conducive to CH_4 production and accretion due to limited routes for efflux. High water table with little subsurface fluctuation only leaves aerenchyma and diffusion as possible conduits for CH_4 and CO_2 flux.

In contrast, dynamic concentrations of CO_2 and CH_4 observed at the near channel subsite were likely due to a hydrologic influence. The near channel subsite exhibited two water table drop and rebounding events; the water table elevation varied from nearly 0 cm on the first sampling date to -25 cm by the third sampling date before rising to +10 cm by the fifth sampling date (Fig. 7b). The dissolved C gas concentrations coincided with these water table dynamics and revealed an accumulation of C gas on the first sampling date, a subsequent decrease in concentration as water table draw down occurred, followed by an increase in CO_2 but not CH_4 gas concentration as the water table rose. The redox dynamics caused by water table fluctuations likely resulted in an imbalance of the dominant microbial respiration processes as the sediments became oxic which diminished the production of CH_4, but not CO_2, during rebounding water table events (Kelley et al. 1995).

The highest CO_2 and CH_4 concentrations observed coincided with the sampling event that spanned a period of complete inundation (on 8/12/15, Table 2). When the water level was above the marsh surface, and had remained so for a period of time (3-5 days), concentrations of CO_2 and CH_4 increased. The minimum CH_4 concentration occurred on 7/29/15 and the minimum CO_2 concentration occurred on 7/12/15. During these two dates, the land surface was newly inundated. This indicates

that there might be a lag in production of CO_2 and CH_4 after inundation. This is especially true for CH_4, which only forms under anaerobic conditions. Lags in the onset of anaerobic metabolism after re-inundation of the sediments has been previously observed in both marshes and wetland soil (Moore and Dalva 1993; Van Der Nat and Middelburg 2000). The decrease in CO_2 concentration observed might also be attributed to a decrease in production rate under anaerobic conditions compared to aerobic conditions. Unlike CH_4, CO_2 does not require anaerobsis and is produced at a faster rate aerobically (Moore and Dalva 1997). Therefore, when inundation occurs, the production rate drops, resulting in less CO_2 in the porewater. However during long periods of inundations, in particular 8/12/15, porewater CO_2 concentrations increased again. We hypothesize that CO_2 becomes trapped within the soil column with limited routes for efflux, increasing the CO_2 concentrations. Gas transport via aerenchyma would be the only means to transport during inundation. However, if the water table level goes lower than the rooting depth, than the gases could be trapped below it.

Seasonal Heterogeneity in The Tidal Marsh

The subsites exhibited similar flux patterns throughout the season, especially in regards to CO_2 flux, with an increase flux in the summer months followed by a subsequent decrease during winter senescence (Fig. 6). The CH_4 seasonal trend is more erratic. Both subsites had low levels of CH_4 punctuated by large one-day increases in flux during the summer growing season and then returning back to a near zero flux. However, unlike CO_2 these spikes do not occur simultaneously and do not exhibit a pattern.

The data collected does not support the hypothesis that areas with less variability (the interior subsite) would experience more of a seasonal flux trend whereas areas with more water table variability (the near channel subsite) would experience fluctuation on a shorter time period. We found that biweekly and weekly measurements are not sufficient to determine lateral spatial heterogeneity of tidally induced gas flux from the soil. In order to observe tidal variation in C gas flux at the ecosystem scale, studies with continuous monitoring of C fluxes using an eddy covariance tower are warranted, which have been used successfully in prior work (Tong et al. 2013; Call et al. 2015; Maher et al. 2015), using high frequency sampling (per second to per hour sampling frequency).

Chapter 5

CONCLUSIONS

Our data suggest that there is lateral and vertical spatial heterogeneity in porewater chemistry resulting from variations in hydrological regimes across the salt marsh. This, in turn, can affect CH_4 and CO_2 production and flux. However, many studies only report in channel and near channel flux values to approximate ecosystem scale CH_4 and CO_2 flux from salt marshes and estuaries as a whole without taking into account spatial gradients (Abril ad Borges, 2004; Poffenbarger et al., 2011; Maher et al., 2013; Middelburg et al., 2014; Call et al., 2015), which may result in the over estimation of CO_2 and an underestimation of CH_4 production and flux. Our data suggest areas that are not consistently inundated are able to produce and release more CO_2 and areas that are consistently inundated without much tidal flushing have the ability to produce more CH_4.

Additionally, depth profiles indicate a large store of CH_4 and CO_2 in the sediment profile that is not reflected in the flux rate observed. There is a large potential for the release of more CH_4 and CO_2 that is stored within the soil column if the hydrological conditions are altered. Draining the marsh would result in a large, one time efflux of both CH_4 and CO_2. Alternatively, if sea level were to rise, resulting in an increase in consistent inundation more uniformly across a marsh (i.e. applying the interior subsite properties to more of the marsh), there would be more potential for CH_4 production. The interplay of hydrology and sediment biogeochemistry should be

considered when attempting to understand the current levels and future dynamics of CO_2 and CH_4 fluxes from salt marshes.

REFERENCES

Abril G, Borges AV (2004) Carbon dioxide and methane emissions from estuaries. In: Tremblay A, Varfalvy C, Roehm, Garneau M (eds) Greenhouse Gas Emissions: Fluxes and Processes, Hydroelectric Resevoirs and Natural Environments. Springer New York, pp 187–207

Abril G, Nogueira M, Etcheber H, et al (2002) Behaviour of organic carbon in nine contrasting european estuaries. Estuar Coast Shelf Sci 54:241–262.

Allen GP, Salomon JC, Bassoullet P, et al (1980) Effects of tides on mixing and suspended sediment transport in macrotidal estuaries. Sediment Geol 26:69–90.

Alperin MJ, Albert DB, Martens CS (1994) Seasonal variations in production and consumption rates of dissolved organic carbon in an organic-rich coastal sediment. Geochim Cosmochim Acta 58:4909–4930.

Avery GB, Shannon RD, White JR, et al (2003) Controls on methane production in a tidal freshwater estuary and a peatland: methane production via acetate fermentation and CO2 reduction. Biogeochemistry 62:19–37.

Bartlett KB, Bartlett DS, Harriss RC, et al (1987) Methane emissions along a salt marsh salinity gradient. Biogeochemistry 4:183–202.

Bartlett KB, Harriss RC, Sebacher DI (1985) Methane flux from coastal salt marshes. J Geophys Res 90:5710–5720.

Bauer JE, Bianchi TS (2011) Dissolved organic carbon cycling and transformation. Treatise Estuar Coast Sci 5:7–67.

Beck M, Dellwig O, Liebezeit G, et al (2008) Spatial and seasonal variations of sulphate, dissolved organic carbon, and nutrients in deep pore waters of intertidal flat sediments. Estuar Coast Shelf Sci 79:307–316.

Call M, Maher DT, Santos IR, et al (2015) Spatial and temporal variability of carbon dioxide and methane fluxes over semi-diurnal and spring–neap–spring timescales in a mangrove creek. Geochim Cosmochim Acta 150:211–225.

Chanton JP, Martens CS, Kelley C a. (1989) Gas transport from methane-saturated, tidal freshwater and wetland sediments. Limnol Oceanogr 34:807–819.

Cline J (1969) Spectrophotometric determination of hydrogen sulfide in natural waters. Limnol Oceanogr 14:454–458.

Drabsch JM, Parnell KE, Hume TM, Dolphin TJ (1999) The capillary fringe and the water table in an intertidal estuarine sand flat. Estuar Coast Shelf Sci 48:215–222.

Fagherazzi S, Wiberg PL, Temmerman S, et al (2013) Fluxes of water, sediments, and biogeochemical compounds in salt marshes. Ecol Process 2:3.

Grill PM, Martens CS (1986) Methane production from bicarbonate and acetate in an anoxic marine sediment. Geochim Cosmochim Acta 50:2089–2097.

Grunwald M, Dellwig O, Beck M, et al (2009) Methane in the southern North Sea: Sources, spatial distribution and budgets. Estuar Coast Shelf Sci 81:445–456.

Holmer M, Kristensen E (1994) Coexistence of sulfate reduction and methane production in an organic-rich sediment. Mar Ecol Prog Ser 107:177–184.

Howarth RW, Merkel S, May N (1984) Pyrite Formation and the Measurement in Salt Marsh Sediments. 29:598–608.

IPCC (2014) Climate Change 2014: mitigation of climate change. Cambridge University Press, New York, NY

Jacinthe PA, Groffman PM (2001) Silicone rubber sampler to measure dissolved gases in saturated soils and waters. Soil Biol Biochem 33:907–912.

Kelley CA, Martens CS, Iii WU, et al (1995) Methane dynamics across a tidally flooded riverbank margin. Am Soc Limnol Oceanogr 40:1112–1129.

Kuivila KM, Murray JW, Devol AH (1990) Methane production in the sulfate-depleted sediments of two marine basins. Geochim Cosmochim Acta 54:403–411.

LaForce MJ, Hansel CM, Fendorf S (2000) Constructing Simple Wetland Sampling Devices. Soil Sci Soc Am J 64:809.

Lovley DR, Phillips EJ (1987) Competitive mechanisms for inhibition of sulfate reduction and methane production in the zone of ferric iron reduction in sediments. Appl Environ Microbiol 53:2636–41.

Maher DT, Cowley K, Santos IR, et al (2015) Methane and carbon dioxide dynamics in a subtropical estuary over a diel cycle: Insights from automated in situ radioactive and stable isotope measurements. Mar Chem 168:69–79.

Maher DT, Santos IR, Golsby-Smith L, et al (2013) Groundwater-derived dissolved inorganic and organic carbon exports from a mangrove tidal creek: The missing mangrove carbon sink? Limnol Oceanogr 58:475–488.

McKeague J a., Day JH (1966) Dithionite- and oxalate-extractable Fe and Al as aids in differentiating various classes of soils. Can J Soil Sci 46:13–22.

Mehra OP (1958) Iron Oxide Removal from Soils and Clays by a Dithionite-Citrate System Buffered with Sodium Bicarbonate. Clays Clay Miner 7:317–327.

Mer J Le, Roger P (2010) Production, oxidation, emission and consumption of methane by soils : A review. Eur J Soil Sci 37:25–50.

Middelburg JJ, Nieuwenhuize J, Iversen N, et al (2014) Methane distribution in European tidal estuaries. Biogeochemistry 59:95–119.

Montalto F a., Parlange J-Y, Steenhuis TS (2007) A simple model for predicting water table fluctuations in a tidal marsh.

Moore T, Dalva M (1993) The influence of temperature and water table position on carbon dioxide and methane emissions from laboratory columns of peatland soils. Eur J Soil Sci 44:651–664.

Moore T, Roulet N (1993) Methane flux: water table relations in northern wetlands. Geophys Res Lett 20:587–590.

Moore TR, Dalva M (1997) Methane and carbon dioxide exchange potentials of peat soils in aerobic and anaerobic laboratory incubations. Soil Biol Biochem 29:1157–1164.

Morse JW, Millero FJ, Cornwell JC, Rickard D (1987) The chemistry of the hydrogen sulfide and iron sulfide systems in natural waters. Earth Sci Rev 24:1–42.

Poffenbarger HJ, Needelman B a., Megonigal JP (2011) Salinity influence on methane emissions from tidal marshes. Wetlands 31:831–842.

Postma D, Jakobsen R (1996) Redox zonation : Equilibrium constraints on the Fe (III)/ SO4-reduction interface. Geochim Cosmochica 60:3169–3175.

Reese BK, Finneran DW, Mills HJ, et al (2011) Examination and refinement of the determination of aqueous hydrogen sulfide by the methylene blue method. Aquat Geochemistry 17:567–582.

Reese BK, Witmer AD, Moller S, et al (2014) Molecular assays advance understanding of sulfate reduction despite cryptic cycles. Biogeochemistry

118:307–319.

Segers R (1998) Methane production and methane consumption : a review of processes underlying wetland methane fluxes. Biogeochemistry 23–51.

Senior E, Lindstrom EB, Banat IM, Nedwell DB (1982) Sulfate reduction and methanogenesis in the sediment of a saltmarsh on the east coast of the United Kingdom. Appl Environ Microbiol 43:987–996.

Smith KA, Ball T, Conen KE, et al (2003) Exchange of greenhouse gases between soil and atmosphere : interactions of soil physical factors and biological processes. Eur J Soil Sci 54:779–791.

Stookey LL (1970) Ferrozine---a new spectrophotometric reagent for iron. Anal Chem 42:779–781.

Teh YA, Silver WL (2006) Effects of soil structure destruction on methane production and carbon partitioning between methanogenic pathways in tropical rain forest soils. J Geophys Res 111:G01003.

Tong C, Huang JF, Hu ZQ, Jin YF (2013) Diurnal variations of carbon dioxide, methane, and nitrous oxide vertical fluxes in a subtropical estuarine marsh on neap and spring tide days. Estuaries and Coasts 36:633–642.

Van Der Nat F-J, Middelburg JJ (2000) Methane Emission from Tidal Freshwater Marshes. Biogeochemistry 49:103–121.

van der Nat F-JW., Middelburg JJ (1998) Seasonal variation in methane oxidation by the rhizosphere of Phragmites australis and Scirpus lacustris. Aquat Bot 61:95–110.

Wachinger G, Fiedler S, Zepp K, et al (2000) Variability of soil methane production on the micro-scale: spatial association with hot spots of organic material and Archaeal populations. Soil Biol Biochem 32:1121–1130.

Weston NB, Dixon RE, Joye SB (2006) Ramifications of increased salinity in tidal freshwater sediments: Geochemistry and microbial pathways of organic matter mineralization. J Geophys Res 111:G01009. doi: 10.1029/2005JG000071

Weston NB, Vile M a., Neubauer SC, Velinsky DJ (2010) Accelerated microbial organic matter mineralization following salt-water intrusion into tidal freshwater marsh soils. Biogeochemistry 102:135–151.

Wilson BJ, Mortazavi B, Kiene RP (2015) Spatial and temporal variability in carbon

dioxide and methane exchange at three coastal marshes along a salinity gradient in a northern Gulf of Mexico estuary. Biogeochemistry 123:329–347.

Winfrey MR, Zeikus JG (1977) Effect of sulfate on carbon and electron flow during microbial methanogenesis in Effect of Sulfate on Carbon and Electron Flow During Microbial Methanogenesis in Freshwater Sediments. Apploed Environ Microbiol 33:275.

Wolanski E (2007) Estuarine Ecohydrology, 1st edn. Elsevier, Oxford, UK